Physics Letters A 382 (2018) 837–845

Contents lists available at ScienceDirect

Physics Letters A

www.elsevier.com/locate/pla

Multi-hump bright solitons in a Schrödinger–mKdV system

Luis A. Cisneros-Ake [a,*], Hugo Parra Prado [b], Diego Joselito López Villatoro [b], R. Carretero-González [c]

[a] Departamento de Matemáticas, ESFM, Instituto Politécnico Nacional, Unidad Profesional Adolfo López Mateos Edificio 9, 07738 Cd. de México, Mexico
[b] Posgrado en Ciencias Fisicomatemáticas, ESFM, Instituto Politécnico Nacional, Unidad Profesional Adolfo López Mateos Edificio 9, 07738 Cd. de México, Mexico
[c] Nonlinear Dynamical Systems Group, Computational Sciences Research Center, and Department of Mathematics and Statistics, San Diego State University, San Diego, CA 92182-7720, USA

ARTICLE INFO

Article history:
Received 3 December 2017
Received in revised form 23 January 2018
Accepted 24 January 2018
Available online 31 January 2018
Communicated by C.R. Doering

Keywords:
Schrödinger–mKdV system
Solitons
Variational approach

ABSTRACT

We consider the problem of energy transport in a Davydov model along an anharmonic crystal medium obeying quartic longitudinal interactions corresponding to rigid interacting particles. The Zabusky and Kruskal unidirectional continuum limit of the original discrete equations reduces, in the long wave approximation, to a coupled system between the linear Schrödinger (LS) equation and the modified Korteweg–de Vries (mKdV) equation. Single- and two-hump bright soliton solutions for this LS–mKdV system are predicted to exist by variational means and numerically confirmed. The one-hump bright solitons are found to be the anharmonic supersonic analogue of the Davydov's solitons while the two-hump (in both components) bright solitons are found to be a novel type of soliton consisting of a two-soliton solution of mKdV trapped by the wave function associated to the LS equation. This two-hump soliton solution, as a two component solution, represents a new class of polaron solution to be contrasted with the two-soliton interaction phenomena from soliton theory, as revealed by a variational approach and direct numerical results for the two-soliton solution.

1. Introduction

The polaron concept, first introduced by Landau [1] and then by Pekar [2], describes how an electron polarizes its surrounding field to deform it and to act as a complete unit, namely a quasi-particle. In the problem of polaron formation, the energy transfer along a crystal lattice (mainly thought of as a lattice of phonons) considers that the electron motion causes a lattice deformation surrounding it, thus producing a local polarization of the lattice, both in the Holstein [3,4] and Davydov [5,6] approaches for on-site non-dispersive and longitudinal dispersive lattice interactions, respectively.

For the polaron motion, or high-polaron, the electron has to drag a cloud of phonons thus virtually increasing its mass and slowing/hampering its motion. Davydov studied this problem in the context of protein chain deformation [7]. In Davydov's approach, the lattice of phonons (or hydrogen bonds) is originally considered in the harmonic limit for longitudinal lattice interactions while the deformation (relative displacement) in the lattice, caused by the electron–lattice interaction, is proportional to the electron's energy. For this type of lattice and electron–lattice interactions, Davydov and Kislukha [8] originally found the self-trapping and propagating mechanisms for the energy transfer along a polypeptide chain of proteins and explained how the transferring electron (described by its wave function) digs its hole in the lattice (as a soliton wave) and drags it at subsonic velocities. The compound wave consisting of a localized wave function plus a soliton wave is so called Davydov's soliton.

Davydov and Zolotaryuk [9], proposed an improvement to his model and considered cubic lattice–lattice interactions as anharmonic longitudinal corrections. These corrections allow the lattice to be valid for larger relative displacements giving rise to new phenomena in the polaron dynamics and preventing from closing the nearest particles each other as opposed in the harmonic limit where nearest particles can pass through each other leading to an unphysical situation. The most remarkable effect is that now the lattice deformation drags the electron and moves it at supersonic velocities, due to the anharmonic lattice interaction proper to shock waves in discrete media [10,11]. The two-directional wave motion of the continuum limit for the energy transfer on a cubic anharmonic discrete medium corresponds to a

* Corresponding author.
E-mail addresses: cisneros@esfm.ipn.mx (L.A. Cisneros-Ake), hparrap1600@alumno.ipn.mx (H. Parra Prado), iq.diego89@gmail.com (D.J. López Villatoro).

https://doi.org/10.1016/j.physleta.2018.01.031
0375-9601/

type of Schrödinger equation coupled to the Boussinesq equation. Although the Schrödinger–Boussinesq system becomes linearly unstable, Davydov et al. [9] and Gaididei et al. [12] found exact solutions traveling at subsonic and supersonic velocities, the so-called Davydov solitons of first and second kind respectively. It is worth mentioning that Gaididei et al. actually found a type of supersonic solution with a two-hump profile that they numerically checked to exist in the corresponding cubic discrete medium resulting in the breathing of the two humps. However, the authors were unable to find the corresponding solution in the continuum medium counterpart due to linear instabilities. They interpreted the leading hump as the one that the anharmonic medium creates when dragging the electron, while the second hump is created as a tunneling effect of such electron. For the stable one-directional continuum limit of cubic anharmonic lattice interactions, Cisneros-Ake et al. [13] found a type of Schrödinger equation coupled to the KdV equation supporting bright and dark solitons of the first and second type as exact solutions of the coupled system. The relevance of this work, in addition to having a linearly stable continuum system, is the finding of a new type of dark soliton solution (of the second kind) having two humps in shape, thus complementing the findings of previous works. Furthermore, the authors of Ref. [13] were unable to find two-hump bright solitons in their LS–KdV system, which is the natural unidirectional stable limit of the LS–Boussinesq system studied by Gaididei et al. [12]. Thus showing remarkable differences between LS–KdV and LS–Boussinesq even though both of them are derived from the same transfer problem along a cubic crystal lattice.

On the other hand, it is important to discuss some of the ideas presented in the fundamental work of Gaididei et al. [12]. They mention that the asymptotic limit of their two-hump supersonic soliton solution (when the two humps are far away each other), in their Schrödinger–Boussinesq coupled system, corresponds to the KdV or Boussinesq two-soliton solution. However, according to the soliton theory, it becomes impossible for an interacting two-soliton solution to become trapped (when they collide) forming an entity of two humps. Thus, a remarkable discovery of Gaididei et al. is that, for their two-hump solution, this kind of mechanism is possible, thanks to the wave function of the coupled system, although they were unable to study it in the continuum system due to linear instabilities and thus were not able to explain the full dynamics.

To complement the ideas developed so far in the previous works, we consider the problem of energy transfer along an anharmonic crystal lattice with quartic lattice–lattice interactions in the Davydov's approach. Following the Zabusky and Kruskal continuum limit for unidirectional propagation, we find a coupled system between the Schrödinger and mKdV equations, as stated in Section 2. Although the KdV and mKdV equations have many similarities like complete integrability and so on, they also present some differences. For instance, mKdV supports breather solutions while KdV does not. Also, the soliton polarity in mKdV can be both positive and negative while in KdV just positive or negative. We will take advantage of this property to look for supersonic polaron solutions in the coupled system under study to find novel families, in the sense of the new proposed nonlinear interactions, of multi-hump solutions not presented in the Schrödinger–KdV system of Ref. [13].

Since our coupled Schrödinger–mKdV system is likely to be not integrable and that no exact solutions can be found following the traveling wave method developed in Refs. [12,13], we thus make use of the variational approach in Section 3 to predict the polaron formation and its dynamics. A further numerical and variational analysis shows that we are actually able to find branches of solitons with one and two humps. We corroborate these findings by employing direct numerical methods in Section 4. In order to describe the full dynamics of the two-hump soliton solutions, we complete our variational approach in Section 5 by considering two-soliton profiles as trial functions to show that the wave function acts as an umbrella that may trap a two-soliton solution of the mKdV equation. We finish our numerical and variational analysis by using a Newton's method in the traveling frame to show the existence of our multi-hump solutions that, after full numerical integration, seem to be dynamically stable. In the last section we present a discussion and conclusions of our findings.

2. Equations of motion

Let us consider the problem of electron transfer along a mechanical crystal lattice with quartic longitudinal interactions in Davydov's approach. Such problem is described by slightly modifying H_{ph} in the well known Hamiltonian $H = H_{el} + H_{ph} + H_{el\text{-}ph}$ provided by Davydov, where:

$$H_{el} = \sum_{n=-\infty}^{\infty} \left[\varepsilon_0 u_n^* u_n - J\left(u_n^* u_{n+1} + u_{n+1}^* u_n\right)\right], \tag{1}$$

$$H_{ph} = \sum_{n=-\infty}^{\infty} \left[\frac{M}{2}\dot{y}_n^2 + \frac{W}{2}\left(y_{n+1} - y_n\right)^2 + \frac{\beta W}{4}\left(y_{n+1} - y_n\right)^4\right], \tag{2}$$

$$H_{el\text{-}ph} = \sum_{n=-\infty}^{\infty} \chi\, u_n^* u_n \left(y_{n+1} - y_{n-1}\right), \tag{3}$$

are the Hamiltonians for the electron, the phonons (lattice), and the electron–phonon interaction, respectively. The physical parameters ε_0 and J are the energy of the electron and the transfer or hopping term for the electron to move from one site to its nearest neighbor. On the other hand, the parameters M and W represent the mass and the elasticity constant for all the phonons, while $\beta > 0$ provides the anharmonicity correction to the lattice–lattice interactions for the longitudinal displacements and χ gives the strength of the electron–phonon interaction.

The corresponding equations of motion, associated to the previous Hamiltonian, are expressed in the form,

$$i\hbar\frac{du_n}{dt} = -J\left(u_{n+1} - 2u_n + u_{n-1}\right) + \chi\left(y_{n+1} - y_{n-1}\right)u_n, \tag{4}$$

$$M\frac{d^2 y_n}{dt^2} = W\left(y_{n+1} - 2y_n + y_{n-1}\right)\left\{1 + \beta\left[\left(y_{n+1} - y_{n-1}\right)^2 - \left(y_n - y_{n-1}\right)\left(y_{n+1} - y_n\right)\right]\right\} + \chi\left(|u_{n+1}|^2 - |u_{n-1}|^2\right), \tag{5}$$

where we have used a gauge transformation to remove the on-site energy term ε_0. u_n represents the probability density function (also called wave function) to describe the electron and y_n measures the relative displacements of the lattice phonons. We recall that the standard Davydov's model, in the harmonic limit, is recovered for $\beta = 0$. We also remark that the decoupled case, $\chi = 0$ in Eq. (5), reproduces the quartic β-FPU (Fermi, Pasta, and Ulam) lattice, which models a chain of hard or rigid interacting particles corresponding to a symmetric potential (which is in contrast to the cubic case, corresponding to soft interacting particles for an asymmetric potential) and it was originally studied to investigate the thermal process in a solid as a finite lattice with appropriate boundary conditions [14]. Thus, our model equations (4)–(5) consider the electron propagation along a rigid crystal lattice. We are interested in the dynamics of this problem in its long wave limit, as developed in the following.

We now consider the unidirectional long wave limit of the model Eqs. (4)–(5). As detailed in the appendix, after applying the

long wave limit with appropriate expansions and rescalings, the continuum limit counterpart to Eqs. (4)–(5) yields:

$$iV\psi_t = -\psi_{xx} + v\psi, \tag{6}$$

$$0 = v_t + 6v^2 v_x + v_{xxx} + \left(|\psi|^2\right)_x, \tag{7}$$

where ψ and v are the continuous, rescaled, analogs of u_n and y_n respectively and V is an effective penalty parameter for the localization of the wave function (see appendix for details). We may observe that solving Eq. (7) for v in terms of the wave function ψ produces in Eq. (6) a Schrödinger equation with nonlinearity $v(\psi)\psi$, while the decoupling of Eq. (7) reduces it to the well known modified Korteweg–de Vries (mKdV) equation. We thus call our model Eqs. (6)–(7) as a Schrödinger–mKdV system.

We now briefly recall some important properties of the mKdV equation. First of all, the scale symmetry allows the solution $-v$ to exist when v is a solution. We will take advantage of this important fact to have coherent solutions in v pointing downwards thus making a proper potential well in the Schrödinger's equation (6) for the wave function ψ. We thus expect to have a chance to support localized coupled (two component) solutions for the system (6)–(7). On the other hand, the mKdV is known to be integrable by means of the inverse scattering method and to support multi-solitons and breather solutions, which may elastically interact between them [17]. In this paper, we seek for the induced possibility of the mKdV soliton's solutions into the coupled system (6)–(7), as it was shown to occur in a similar coupled system [13].

Our first attempt to find exact solutions to Eqs. (6)–(7) is to try the traveling wave formalism. To this end, the substitutions $\psi(x,t) = f(x-ct)\,e^{i(kx-\beta t)}$ and $v(x,t) = g(x-ct)$ reduce to the ordinary differential equations (ODEs), similar to a quartic Hénon–Heiles system,

$$f'' = f\left(k^2 - \beta V + g\right), \tag{8}$$

$$g'' = cg - 2g^3 - f^2, \tag{9}$$

where the equation for g has been integrated once for zero conditions at infinity (soliton's condition). It is important to notice that the unidirectional limit and now the traveling frame modify the overall velocity of propagation to $\left(1 + ch^2/24\right)v_s$, thus having supersonic motion for $c > 0$, sonic motion if $c = 0$ and subsonic one for $c < 0$. Now, one may try either the usual techniques in dynamical systems to integrate (8)–(9) [18] or at least to find exact solutions by an ODE reduction for an appropriate compatibility condition $f = \mathcal{F}(g)$, as it was possible to do in a Schrödinger–KdV system [13] or in an equivalent Schrödinger–Boussinesq system by using a proper change of variables in the traveling coordinate [10,11]. However, a quick analysis shows the impossibility to proceed with either of these techniques because the parameters and nonlinear interactions in Eqs. (8)–(9) do not meet the proper conditions needed to perform the relevant integrations.

In order to look for approximate localized coherent solutions to our system (6)–(7), we proceed by means of variational techniques.

3. Variational approach

The variational approximation is based on the extremization of the Lagrangian (associated to the equations of motion) averaged on a proper family of trial functions or ansatz [19]. The extrema of the average Lagrangian are then evaluated in terms of the Euler–Lagrange equations for the wave parameters describing the family of trial functions. Thus, to follow the variational approach, we first need to derive our equations of motion (6)–(7) from a variational principle. To this end, we introduce the change of variables $v = \varphi_x$ and make use of the inverse problem of calculus of variations to directly cast the associated Lagrangian:

$$L = \int_{-\infty}^{\infty} \mathcal{L}\,dx, \tag{10}$$

$$\mathcal{L} = \varphi_x\varphi_t + \varphi_x^4 - \varphi_{xx}^2 - iV\left(\psi_t\psi^* - \psi_t^*\psi\right) + 2|\psi_x|^2 + 2\varphi_x|\psi|^2.$$

As it was discussed above, the decoupling of Eqs. (6) and (7) reduces to a type of nonlinear Schrödinger equation and to a mKdV equation. Then, to take into account appropriate trial functions, we should consider the soliton's profile that both equations sustain separately. That is

$$\varphi(x,t) = A\arctan\left(\tanh\left[w\left(x-\xi(t)\right)\right]\right), \tag{11}$$

$$\psi(x,t) = B\,\mathrm{sech}\left[w\left(x-\xi(t)\right)\right]e^{i\left[k\left(x-\xi(t)\right)+\Phi(t)\right]}. \tag{12}$$

We may notice that functions (11) and (12) represent coupled coherent profiles having a localized shape with the *same* width w and position $\xi(t)$. We stress that the amplitude parameters A and B and the common width w are not considered as functions of time, since in their variations we are just interested in their equilibrium values where the extreme of the average Lagrangian is reached. On the other hand, position $\xi(t)$ and phase $\Phi(t)$ are indeed functions of time so to consider the dynamics of the coherent traveling wave, while the phase's velocity k is also considered as a constant to have a solitary wave traveling at a constant velocity. We are now ready to develop the variational formalism. We start our procedure by averaging (integrating along x) the Lagrangian (10) with the family of trial functions (11)–(12) to obtain:

$$L = -A^2 w\xi' + \frac{2}{3}A^4w^3 - \frac{4}{3}A^2w^3 - \frac{4}{w}VB^2\left(k\xi' - \Phi'\right) + \frac{4}{3}wB^2 + \frac{4}{w}B^2k^2 + 2(\pi-2)AB^2. \tag{13}$$

Next, we find the equations of motion for the wave parameters by using the Euler–Lagrange equations for the above average Lagrangian. This process yields the following simplified system of equations:

$$\delta A: 0 = -2Aw\xi' + \frac{8}{3}A^3w^3 - \frac{8}{3}Aw^3 + 2(\pi-2)B^2, \tag{14}$$

$$\delta B: 0 = \frac{2}{3}wB - \frac{2}{w}VB\left(k\xi' - \Phi'\right) + \frac{2}{w}Bk^2 + (\pi-2)AB, \tag{15}$$

$$\delta w: 0 = -A^2\xi' + 2A^4w^2 - 4A^2w^2 + \frac{4}{w^2}VB^2\left(k\xi' - \Phi'\right) + \frac{4}{3}B^2 - \frac{4}{w^2}B^2k^2, \tag{16}$$

$$\delta k: k = \frac{V}{2}\xi'. \tag{17}$$

Since we must have a two-parameter family of solutions, variations in ξ and Φ do not provide extra conditions but only conservation equations, which we do not display here. Thus, Eqs. (14)–(17) are a complete system for the wave parameters provided that two of them, say w and ξ', are given.

To find appropriate relationships between the wave parameters, in terms of the two free parameters w and ξ', we may first cancel Φ' out from the expressions for δB and δw to get:

$$6(\pi-2)AB^2 + 8wB^2 + 6A^4w^3 - 3A^2w\left(\xi' + 4w^2\right) = 0. \tag{18}$$

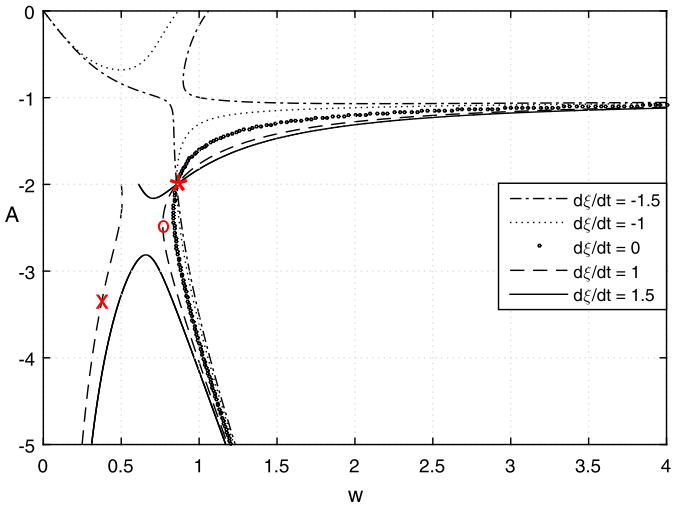

Fig. 1. Dispersion relation $A = A(w)$ obtained from Eq. (20) for $V = 1$ and different velocities corresponding to: $\xi' = -1.5$ (dash-dot curves), $\xi' = -1$ (dot curves), $\xi' = 0$ (dotted curve), $\xi' = 1$ (dashed curves), and $\xi' = 1.5$ (solid curves). The marks "x", "o", and "$*$" are reference points where the transition from a one-hump (above marks) to a two-hump (below the marks) solution takes place.

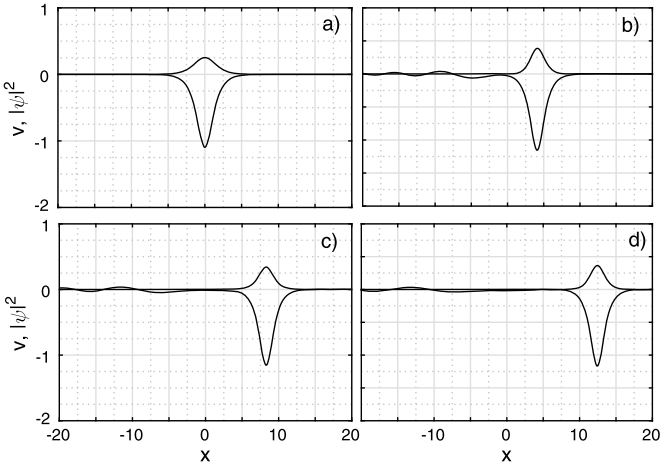

Fig. 2. Evolution of a one-hump profile predicted by the variational approximation. Full numerical evolution of an initial condition given by the variational approximation using the one-hump ansatz (11)–(12) for parameters $V = 1$, $w = 0.5059$, $A = -2.1684$ and $\xi' = 1$. a) $t = 0$, b) $t = 4$, c) $t = 8$ and d) $t = 12$. In this and all subsequent figure the top and bottom waveforms correspond, respectively, to $|\psi(x,t)|^2$ and $v(x,t)$.

Using this last expression, jointly with the equation for δA, to remove ξ', yields

$$B^2 = \frac{2A^2w^3\left(4 - A^2\right)}{3\left(\pi - 2\right)A + 8w}, \tag{19}$$

which provides an involved relation between the amplitudes B and A, equivalent to the one found in Davydov's soliton [9] where the wave amplitude A is proportional to the square of the wave function amplitude B. We also remark that the amplitude B of the wave function ψ vanishes precisely at $A = 0$ and $A = -2$ [provided that $3\left(\pi - 2\right)A + 8w \neq 0$], which reproduces the trivial solutions for the PDE system (6)–(7): $\psi = 0$, $v = 0$ and $\psi = 0$, $v = -2w\,\mathrm{sech}\left[2w\left(x - \xi(t)\right)\right]$ corresponding to the zero solution and to the zero solution plus the mKdV soliton, respectively. We finally substitute back expression (19) into Eq. (18) to get a nonlinear dispersion relationship between the wave parameters w, A and ξ' of the form:

$$\xi' = \frac{4w^2(4 - A^2)}{9(\pi - 2)A + 24w}\left[3\left(\pi - 2\right)A + 4w\right] + 2A^2w^2 - 4w^2. \tag{20}$$

We thus have shown so far that the two free parameters, the velocity ξ' and the solitons' width w, determine the evolution of the rest of the parameters. Fig. 1 precisely displays this fact: given a velocity value, ξ', the dispersion relation $A = A(w)$ is obtained. Hence, if the width w is also given, then the amplitude A is obtained and thus from (19) the other amplitude B is also determined. The phase velocity k is then determined from (17) while Φ is obtained from, say, (15).

Let us analyze in more detail the features depicted in Fig. 1. The first remarkable observation is the appearance of two branches of solutions for any positive and negative value of the velocity (except for $\xi' = 0$ where just one branch occurs). In each case, one of the branches arises or starts either from the trivial zero–zero solution corresponding to $A = 0$, $w = 0$ [and thus $B = 0$, see Eq. (19)] or the zero solution plus the mKdV soliton solution corresponding to $A = -2$ and $w < \frac{3}{4}(\pi - 2)$ (thus once again $B = 0$). On the other hand, we may notice that Eq. (19) has an undefined limit at $A^* = -2$ and $w^* = \frac{3}{4}(\pi - 2)$ producing non-zero values for B, depending on the direction we approach A^* and w^*. Such direction is determined, according to Fig. 1, from the curve $A = A(w)$ obtained for a given velocity value ξ'. Fig. 1 also shows that one of the two branches, obtained from any velocity ξ', crosses the point A^*, w^*. We thus have here a type of special solution where a fixed mKdV soliton with amplitude A^* and width w^* may travel with *any* velocity (positive or negative) coupled to the corresponding wave function ψ. We will numerically analyze this case in the next section.

The last observation we make about Fig. 1 concerns the kind of bifurcation diagram it represents. All the branches displayed in the figure seem to have a turning point, in addition to the fact that they appear in pairs. We may actually observe that, as the velocity increases from negative values (say, $\xi' = -1.5$), a first branch interchange occurs close to $\xi' = -1.25$ then a branch is lost at $\xi' = 0$ and it appears again for $\xi' > 0$. Finally, as the velocity increases further, there is another branch exchange at approximately $\xi' = 1.25$.

We now study in detail the different scenarios provided by the diagram of Fig. 1 in order to discern all the solution types predicted by the variational approach.

4. Dynamical evolution of the soliton solutions

We now numerically study our PDE system (6)–(7) for different initial conditions taken from the variational predictions of Fig. 1. We make use of the pseudo spectral method (PSM) [20] in space and a fourth order Runge–Kutta method in time to numerically solve the Eqs. (6)–(7). Large enough spatial domains are considered to avoid the possibility of wave transfer along the periodic boundary inherent in the PSM.

We start our numerical analysis of solutions by considering a typical one-hump soliton solution (bright soliton coupled to mKdV soliton) as stated by the trial functions (11)–(12). We recall that in the electron transfer problem, normalized wave functions have to be considered in the form $\int_{-\infty}^{\infty}|\psi(x,t)|^2dx = 1$ which imposes, according to Eq. (12), the parameter constraint $2B^2 = w$. This constraint, for a given velocity of propagation, ξ', corresponds to a particular point in one of the two branches displayed in Fig. 1. We thus consider the velocity of propagation $\xi' = 1$ and the model parameter $V = 1$ to variationally predict $A = -2.1684$ and $w = 0.5059$ for an initial normalized wave function. The rest of the wave parameters are obtained as described in the previous section. Fig. 2 shows how the initial condition obtained from the

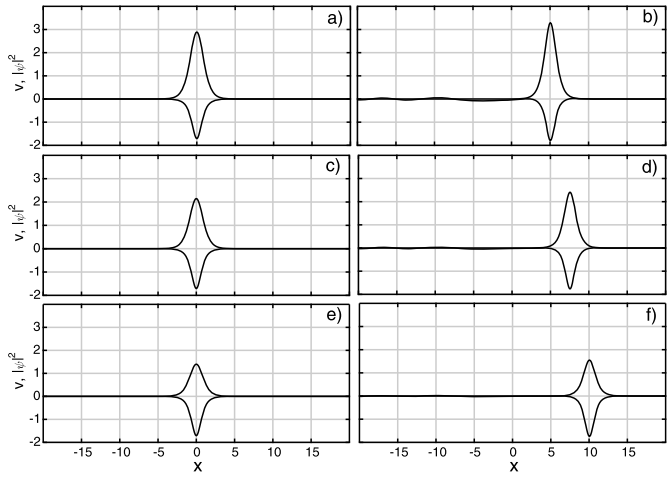

Fig. 3. Evolution of one-hump profiles for different velocities, but the same model parameters, predicted by the variational approximation. Full numerical evolution of initial conditions given by the variational approximation using the one-hump ansatz (11)–(12) for parameters $V = 1$, $A = A^* = -2$, $w = w^* = \frac{3}{4}(\pi - 2)$ for a)–b) $B^2 = 2.892$, $\xi' = 1$, c)–d) $B^2 = 2.15$, $\xi' = 1.5$, and e)–f) $B^2 = 1.4$, $\xi' = 2$. a), c) and e) at $t = 0$ while b), d) and f) at $t = 5$.

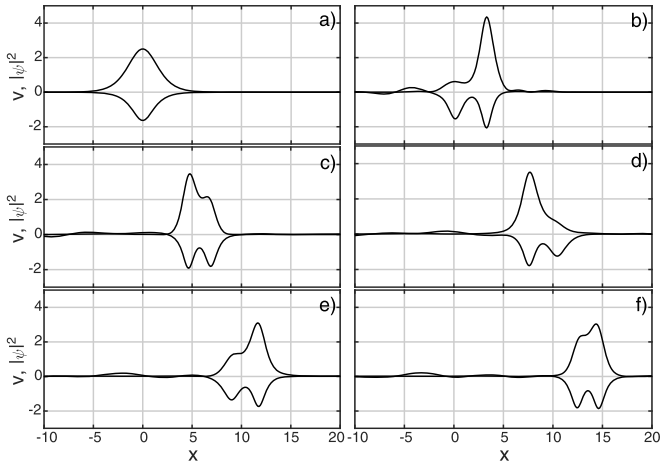

Fig. 4. Initial one-hump profile evolving into a two-hump one. Full numerical evolution of an initial condition given by the variational approximation using the one-hump ansatz (11)–(12) for parameters $V = 1$, $w = 0.5$, $A = -3.2755$ and $\xi' = 1.5$. a) $t = 0$, b) $t = 2$, c) $t = 4$, d) $t = 6$, e) $t = 8$ and f) $t = 10$.

variational approach evolves in time. A very small transient occurs initially to adjust the profiles to the numerically exact one. Such transient generates a train of linear waves traveling backwards from the leading localized wave. Fig. 2b) shows indeed the transient effect since, as it can be observed by comparing with Fig. 2a), the amplitude and width slightly change as well as the numerical velocity. After the initial transient, the wave profiles preserve their shape and the normalization condition up to an accepted numerical error due to the PSM approximation, see Figs. 2b)–d). This corroborates the validity of the variational prediction to describe the one-hump traveling profiles. We will ignore henceforth the normalization condition and take the point of view of nonlinear optics to analyze the whole branches displayed in Fig. 1.

As Fig. 1 shows, a special case arises at the particular parameter values $(w, A) = (w^*, A^*)$ for any velocity ξ'. We now discuss this case. We consider the velocities $\xi' = 1$, 1.5 and 2 and their corresponding branches $A = A(w)$ crossing at (w^*, A^*) along which we determine the directional limits of Eq. (19) to find $B^2 = 2.892$, $B^2 = 2.15$ and $B^2 = 1.4$, respectively. The numerical evolution of these three initial conditions are displayed in Fig. 3. The key point of this example is that the same mKdV soliton with wave parameters w^* and A^* drags different wave functions ψ with corresponding *different* velocities. It is actually observed that faster coupled solutions correspond to smaller wave functions. Thus, from the physical point of view, a transferring electron with different probability density digs the same hole at the expense of moving faster or slower.

Let us now consider a different set of wave parameters. As it was discussed in the previous section, one of the branches $A = A(w)$ generated by the velocity value $\xi' = 1.5$ is parabolic in shape and pointing downwards. We take a value of w in this branch, say, $w = 0.5$ thus obtaining $A = -3.2755$ and then the rest of the wave parameters are determined as before yielding a predicted initial condition. The corresponding numerical evolution for this initial condition is shown in Fig. 4. Figs. 4a)–b) display an interesting phenomenon for this initial condition: an initial one-hump profile, with enough mass, evolves into a two-hump solitary wave solution [see Figs. 4b)–f)] showing a new type of solution to the coupled system (6)–(7). The two humps breath alternating their minima/maxima along the evolution.

For all the branches displayed in Fig. 1, we have approximately identified the critical point along the branches where a transition from one hump to two humps occurs, see cross, circle and asterisk marks: one-hump profiles are found above such marks while two-hump profiles are found below the marks. In the case of the velocity $\xi' = 1.5$, there is no mark since the whole branch (parabolic in shape and pointing downwards) is a branch of two-humps solutions, while both branches associated to the velocity $\xi' = 1$ have marks (cross and circle respectively). This suggests that, as the velocity increases, these two marks coalesce (bifurcate) to form the parabolic branch of $\xi' = 1.5$, thus qualitatively causing an exchange of branches.

On the other hand, since the anharmonic medium is responsible for the supersonic motion of the two component solution (wave function plus mKdV soliton), the mKdV soliton splits into two humps first and then it forces the wave function to generate a second hump to finally drag it. Our interpretation is that the two humps in the mKdV soliton correspond to a two-soliton solution in the mKdV equation trapped by the wave function, which in turn acts as an umbrella to keep trapped both mKdV solitons together. We name this phenomenon as *the umbrella effect*. Note that without this umbrella effect, the nonlinear interaction between the two mKdV solitons would force them to separate. Fig. 4 also shows a type of bounce-exchange interaction between the two humps although we have identified for other initial conditions a type of merge–split interaction between the humps (not displayed here), which are well known to occur in the soliton interaction for the mKdV equation, see [21]. It is important to note at this stage that the two-hump soliton solution just described remarkably differs from the ones previously found in Refs. [11,12], mainly due to the dynamics impregnated by the mKdV solitons on the two humps. We will justify in the next section some of the phenomena observed in Fig. 4.

5. Bound two-soliton solutions

We now give a more detail explanation of the umbrella effect. According to the numerical evidence shown in the previous section, we must consider the two-soliton interaction of the two component one-hump solutions. We do this with the help of the variational approach, as developed in Section 3. We thus consider the modified trial functions,

$$\varphi(x,t) = A \arctan\left(\tanh\left[\alpha\,(x - \xi(t))\right]\right) + B \arctan\left(\tanh\left[\beta\,(x - \eta(t))\right]\right), \tag{21}$$

$$\psi(x,t) = C\,\mathrm{sech}\left[\alpha\,(x-\xi(t))\right] e^{i\left[v_1(x-\xi(t))+\Phi(t)\right]} + D\,\mathrm{sech}\left[\beta\,(x-\eta(t))\right] e^{i\left[v_2(x-\eta(t))+\rho(t)\right]}, \tag{22}$$

corresponding to the superposition of two of the localized solutions introduced in Section 3. The average Lagrangian for this two-humped ansatz yields:

$$\begin{aligned} L = & -A^2\alpha\xi' - AB\alpha\beta\left(\xi'+\eta'\right) I_1 - B^2\beta\eta' + \frac{2}{3}A^4\alpha^3 \\ & +4A^3B\alpha^3\beta I_2 \\ & +6A^2B^2\alpha^2\beta^2 I_3 + 4AB^3\alpha\beta^3 I_4 + \frac{2}{3}B^4\beta^3 - \frac{4}{3}A^2\alpha^3 \\ & -8AB\alpha^2\beta^2 I_5 - \frac{4}{3}B^2\beta^3 + \frac{4C^2}{\alpha}\left[-V\left(v_1\xi'+\Phi'\right)+v_1^2\right] \\ & -2CD\left[V\left(v_2\eta'-\rho'\right)+V\left(v_1\xi'-\Phi'\right)-2v_1v_2\right] I_6 \\ & +2CD\beta\left(V\eta'-2v_1\right) I_7 + \frac{4}{3}C^2\alpha + \frac{4}{3}D^2\beta \\ & -2CD\alpha\left(V\xi'-2v_2\right) I_8 + \frac{4D^2}{\beta}\left[-V\left(v_2\eta'-\rho'\right)+v_2^2\right] \\ & +4CD\alpha\beta I_9 + 2\left(\pi-2\right)AC^2 + 2\left(\pi-2\right)BD^2 + 2AD^2\alpha I_{10} \\ & +2BC^2\beta I_{11} + 4ACD\alpha I_{12} + 4BCD\beta I_{13}, \end{aligned} \tag{23}$$

where the I_j are overlapping integrals due to the two-soliton interaction. Among these, the important ones for our purposes [see Eq. (24) below] are I_1, I_6, I_7 and I_8 which take the form

$$I_1 = \int_{-\infty}^{\infty} \mathrm{sech}\left[2\alpha z\right]\mathrm{sech}\left[2\beta(z+\theta)\right] dz,$$

$$I_6 = \int_{-\infty}^{\infty} \mathrm{sech}\left[\alpha z\right]\mathrm{sech}\left[\beta(z+\theta)\right]\cos\gamma\, dz,$$

$$I_7 = \int_{-\infty}^{\infty} \mathrm{sech}\left[\alpha z\right]\mathrm{sech}\left[\beta(z+\theta)\right]\tanh\left[\beta(z+\theta)\right]\sin\gamma\, dz,$$

$$I_8 = \int_{-\infty}^{\infty} \mathrm{sech}\left[\alpha z\right]\tanh\left[\alpha z\right]\mathrm{sech}\left[\beta(z+\theta)\right]\sin\gamma\, dz,$$

where $\gamma = \Delta_v z + v_2\theta + \Delta_\rho$, $\theta = \xi - \eta$ is the relative position of the two solitons, $\Delta_v = v_2 - v_1$ is the velocity difference while $\Delta_\rho = \rho - \Phi$ is the phase difference between the two wave functions. We recall that the particular case $B = D = 0$ reduces to the previous Lagrangian (13) for the one soliton of the two component solution, while $C = D = 0$ reduces to the two-soliton interaction for the mKdV equation. Thus, the effects of both particular cases should be considered by our variational approximation in order to give an explanation for the two-hump solution. Since we expect that the two-soliton interaction in mKdV is responsible for the two-hump formation in the two component solution of Eqs. (6)–(7), we are thus interested in the variational evolution of the relative soliton displacement θ. In order to do this, we combine the variations of L in ξ and η (not shown here) to find the simplified expression:

$$F(\theta) = AB I_1'(\theta) + CDV(v_1+v_2) I_6'(\theta) - CD\beta V I_7'(\theta) + CD\alpha V I_8'(\theta) = 0, \tag{24}$$

where the integrals I_1, I_6, I_7 and I_8 are numerically estimated by numerical quadratures as a function of θ for given values of α, β, Δ_v, v_2 and Δ_ρ.

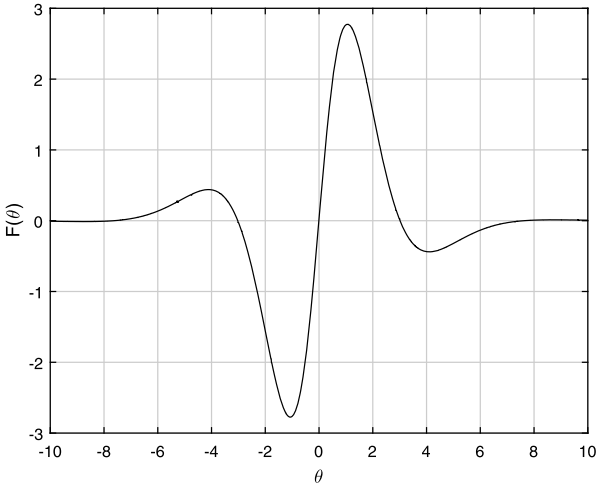

Fig. 5. Graph of $F(\theta)$ obtained from Eq. (24) for the wave parameters $\beta = 1.0728$, $\alpha = 0.782$, $A = -2.25$, $B = -1.75$, $C = 1.89$, $D = 1.65$, $\Delta_v = 0.25$, $v_2 = 0.75$, and $\Delta_\rho = 0$. The zeros for F correspond to stationary solutions of our variational approximation.

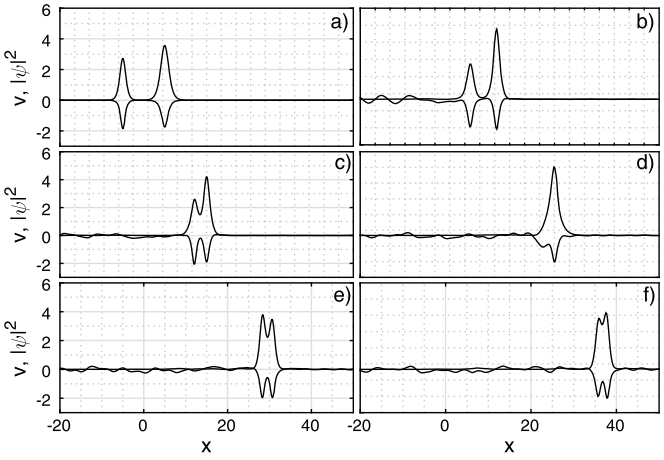

Fig. 6. Collision of two solitons leading to a bound two-soliton solution. The two initial solitons correspond to the profiles described in Eqs. (21)–(22) for the parameters $\beta = 1.0728$, $\alpha = 0.782$, $A = -2.25$, $B = -1.75$, $C = 1.89$, $D = 1.65$, $\eta' = 1.5$, $\xi' = 1$, $\xi = 5$ and $\eta = -5$. a) $t = 0$, b) $t = 7$, c) $t = 10.5$, d) $t = 20$, e) $t = 23.5$ and f) $t = 29.75$.

Fig. 5 displays the graph of $F(\theta)$ for a particular combination of the parameters. It is straightforward to check that $F(\theta)$ is an odd function and, thus, there are three symmetric type of equilibria in θ (the relative positions of the two solitons). One is at $\theta = 0$, which corresponds to the case when the two solitons are on top of each other and thus the two-hump ansatz effectively reduces to a one-hump profile. The other two equilibria (symmetric with respect to zero) occur at approximately $\theta = \pm 3$. These correspond to genuine two-hump profiles composed by a trapped two-mKdV soliton. The emergence of these two-hump profiles can be explained as follows: for an initial condition with appropriate wave parameters corresponding to two (well) separated solitons, the solitons can become trapped by the wave function $|\psi|^2$ that plays the role of the umbrella to bind these two solitons together.

We illustrate this binding phenomenon in Fig. 6 where we consider the numerical evolution of two initially separated solutions as described by Eqs. (21)–(22) with $\xi = 5$, $\eta = -5$, $\eta' = 1.5$, $\xi' = 1$, and all other parameters corresponding to the ones used in Fig. 5. The initial separation is $\theta = \xi - \eta = 10$ units corresponding to a *larger* separation than the one predicted by the non-trivial zeroes of $F(\theta)$ where the separation should be close to $\theta = 3$. As

the figure shows, the two solitons initially evolve (almost) freely as they are well separated. However, as they get closer (leftmost soliton was initialized with a larger velocity than the rightmost one), they collide and as a result we obtain a *bound* two-hump solution with an internal distance between the humps of approximately 3 units which is precisely the distance predicted by our variational method for the parameters used in this example. It is remarkable that the umbrella effect is able to bind together the colliding solitons through the ejection of undesired radiation towards the background. This is a strong indication that the umbrella effect is rather strong (stable) and is even able to trap solitons that where initialized far away from each other provided that at some point they got close to each other. It would be interesting to study in more detail the conditions necessary for trapping two colliding solitons as it is clear that two solitons with very different velocities will not be able to be trapped by the umbrella effect and will rather collide in a manner akin to pure mKdV solitons. This avenue for future investigation is currently under consideration and will be reported in a future publication.

It is important to note that the resulting trapped two-hump solutions depicted in Fig. 6 (see last panel) and in Fig. 4 correspond to an alternating internal breathing between the two humps. Capturing these breathing solutions in the numerics would involve finding periodic solutions in a co-moving reference frame. This task would require to setup a Floquet-type analysis in the co-moving frame. This falls outside the scope of the present manuscript. Nonetheless, it is possible to seek for stationary, i.e. non-breathing, multi-hump solutions by use of a standard Newton method applied in a co-moving reference frame. Therefore, let us first rewrite our initial model Eqs. (6)–(7) in the traveling moving frame $z = x - ct$, $\tau = t$:

$$iV\psi_\tau - iVc\psi_z = -\psi_{zz} + v\psi,$$
$$0 = v_\tau - cv_z + 6v^2 v_z + v_{zzz} + \left(|\psi|^2\right)_z.$$

The stationary state of the wave function ψ requires to evolve its phase in the form: $\psi = \phi(z)e^{i\mu\tau}$ where μ corresponds to its (temporal) frequency, while for v we only require $v_\tau = 0$. These two considerations simplify the previous equations to

$$-V\mu\phi - iVc\phi_z = -\phi_{zz} + v\phi, \tag{25}$$
$$0 = -cv + 2v^3 + v_{zz} + |\phi|^2, \tag{26}$$

where Eq. (26) has been integrated once with respect to z using zero conditions at infinity. Equations (25)–(26) correspond to an ODE system which may numerically be solved using a Newton's method after approximating the spatial derivatives using second order finite differences with spacing h:

$$-V\mu u_n + \frac{Vc}{2h}(w_{n+1} - w_{n-1}) = -\frac{1}{h^2}(u_{n-1} - 2u_n + u_{n+1}) + v_n u_n,$$
$$-V\mu w_n - \frac{Vc}{2h}(u_{n+1} - u_{n-1}) = -\frac{1}{h^2}(w_{n-1} - 2w_n + w_{n+1}) + v_n w_n,$$
$$0 = -cv_n + 2v_n^3 + \frac{1}{h^2}(v_{n-1} - 2v_n + v_{n+1}) + u_n^2 + w_n^2,$$

and where the wavefunction has been split into its real and imaginary parts: $\phi_n = u_n + iw_n$.

In order to find stationary two-hump profiles, we apply the above Newton's method to an initial condition obtained from the variational approach in a region of the parameters where the evolution tended to a breathing two-hump profiles. Namely, we take parameter values on the branches depicted in Fig. 1 *below* the marks where two-hump solutions have been observed. For example, we depict in Fig. 7 one such scenario. This figure suggests that, in addition to breathing alternating two-hump profiles, the umbrella effect is also capable of supporting symmetric configurations. The figure also suggests that, for the chosen parameter values, this symmetric two-hump profile is stable (we have integrated the system for longer times and the profile remains stable). An interesting question that arises in this case of a stable, symmetric, two-hump profile is to how nearby orbits would evolve. Fig. 8 depicts the evolution of an initial condition corresponding to a perturbed symmetric two-hump profile. The perturbation is induced by changes in the height and/or width of the original solution. The figure suggests that as the symmetric one-hump profile is perturbed, the system picks a nearby solution corresponding to a *breathing*, i.e. asymmetric, profile. This picture is consistent with the symmetric solutions being neutrally stable centers around which periodic solutions, corresponding to the asymmetric breathing profiles, coexist.

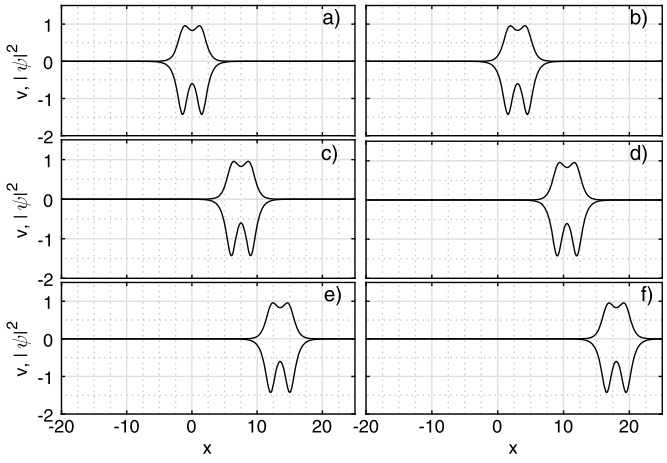

Fig. 7. Traveling, symmetric, two-hump solution. Full numerical evolution for an initial condition obtained via Newton iteration on a seed profile given by Eqs. (11)–(12) with parameters provided by the variational approximation corresponding to $w = 0.395$, $A = -4$, $B = 1.5$, $\xi' = 1.5$ and $V = 1$. a) $t = 0$, b) $t = 2$, c) $t = 5$, d) $t = 7$, e) $t = 9$, f) $t = 12$.

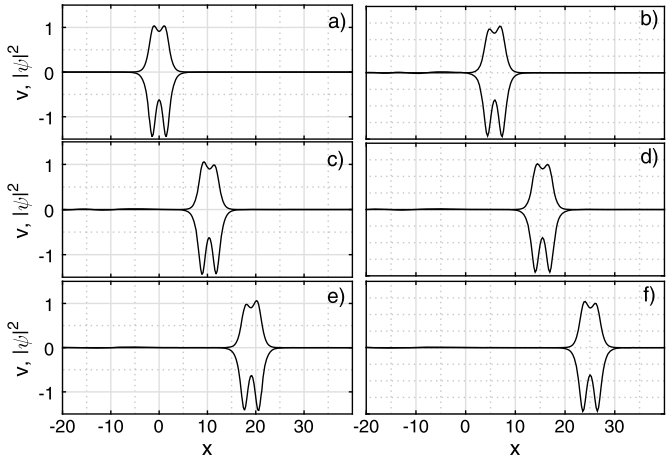

Fig. 8. Evolution corresponding to a perturbed symmetric two-hump profile. The original (unperturbed) profile correspond to the solution obtained through Newton iterations starting with a seed provided by our variational method on the ansatz (11)–(12) for $w = 0.395$, $A = -4$, $B = 1.5$, $\xi' = 1.5$, $V = 1$, and $\mu = 1.413$. a) $t = 0$, b) $t = 4$, c) $t = 7$, d) $t = 10.5$, e) $t = 13$, f) $t = 17$.

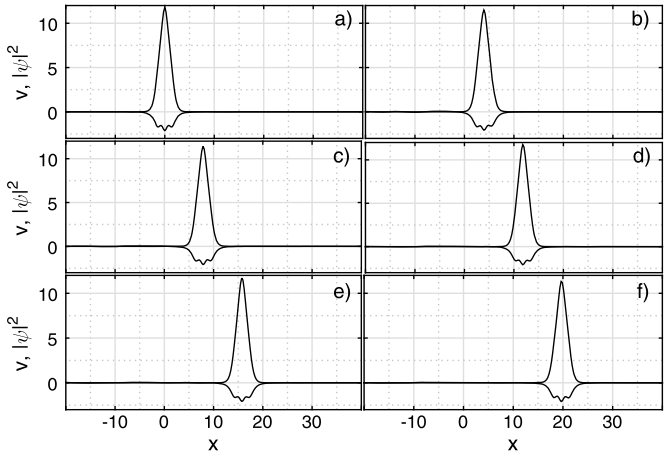

Fig. 9. Stable, symmetric, three-hump profile. The initial condition was obtained from seeding a Gaussian profile in the Newton's method for $V = 1$, $c = 1.5$, and $\mu = 1.6994$. a) $t = 0$, b) $t = 4$, c) $t = 8$, d) $t = 12$, e) $t = 16$, f) $t = 20$.

Finally, we depict in Fig. 9 the stable evolution of a three-hump profile obtained through Newton's iterations on an initial Gaussian seed. Interestingly, the stable solution contained three humps in v and only one hump in ψ. This example suggest the possible existence (and stability) of more complex profiles with combinations of multiple humps in the two components. A detailed stability (and bifurcation) analysis for these symmetric and asymmetric multi-hump solutions as the physical parameters (i.e. V) and the main wave parameters (μ and c) are varied falls outside of the scope of the current work and it is currently under investigation and will be reported in a future publication.

6. Discussion and conclusions

We have studied the problem of electron transfer along an anharmonic quartic medium. In the long wave approximation for unidirectional wave propagation, an effective model that couples the Schrödinger and the mKdV equations was found. We showed that in addition to the standard soliton solution (a bright soliton for Schrödinger coupled to a mKdV soliton), novel type of multi-hump soliton solutions also exist. We studied in some detail soliton solutions consisting of two-humps in both components and we ascribed their emergence by a trapping mechanism whereby the Schrödinger wavefunction plays the role of an "umbrella" that binds the two mKdV solitons together. We found that this umbrella effect was capable of supporting stable, symmetric, two-hump profiles corresponding to stationary states in a co-traveling frame. Perturbations off of these symmetric solutions tended to produce asymmetric two-hump profiles with internal, alternating, breathing between the two humps. Interestingly, we also observed that "soft" collisions between two individual one-hump profiles produced bound two-hump solutions through the trapping umbrella effect.

To follow the main characteristics of these solutions, we employed one- and two-hump ansatze within the variational approximation methodology and found that, for fixed model parameters, a plethora of one- and two-hump solutions coexist for different wave parameters (width, height, and speed). The obtained solutions were found to be stable for the chosen parameters values. An exception was the case of profiles traveling backwards (negative velocity). In that case, due to their strong interaction, with the linear dispersed waves, they were found to be unstable and were eventually destroyed by the linear emitted radiation.

There are several avenues along which the current work could be extended. The immediately one could be to consider the discrete original counterpart, as it was studied in Ref. [22] for the cubic case, to see if the type of multi-hump solutions exist there or if new phenomena take place. Also, for instance, a detailed stability, i.e. bifurcation, analysis for the main multi-hump solutions could reveal interesting bifurcation phenomena. This analysis would require to study the Floquet stability for the breathing, periodic, profiles. Also interesting would be to study in detail the scattering-like events for colliding one-soliton solutions and to determine conditions for how "soft" a collision has to be for the umbrella effect to be able to trap two (or more) solitons. Another open question concerning our model equations is the existence of similar multi-hump solutions in the case of effective repulsive nonlinearity that could potentially give rise to dark soliton solutions. Finally, extensions to two-dimensional systems could give rise to interesting dynamics involving structures with vorticity.

Acknowledgements

L.A. Cisneros-Ake dedicates this paper to the memory of his mentor, colleague and friend professor A.A. Minzoni, from whom he first heard the word soliton and who recently passed away. This research has been sponsored by COFAA–IPN and IPN-CGPI-20170867. R.C.G. acknowledges support from NSF-PHY-1603058. We also thank the anonymous referees for their insightful comments.

Appendix A. Unidirectional continuum limit

In order to obtain the continuous limit analog to the discrete model given in Eqs. (4)–(5), let us follow Ref. [13]. We start by introducing the bulk physical parameters in terms of the lattice spacing h:

$$\frac{M}{h} = \bar{\eta}, \quad Wh = \zeta, \quad \frac{2}{h}\chi = \tilde{\chi},$$

where $\bar{\eta}$ is the linear mass density of the phonons, ζ is the spring constant for a piece of chain of unit length and $\tilde{\chi}$ is the scaled energy resulting from a molecular displacement of one lattice constant in the linearized exciton field [15]. We now consider the asymptotic limit of the system (4)–(5) corresponding to second order Taylor expansions for finite, but small, h to obtain:

$$i\hbar u_t = -Jh^2 u_{xx} + \tilde{\chi} h^2 y_x u,$$
$$\frac{\bar{\eta}}{\zeta} y_{tt} = y_{xx} + 3h^2\beta y_x^2 y_{xx} + \frac{h^2}{12} y_{xxxx} + \frac{\tilde{\chi} h}{\zeta}\left(|u|^2\right)_x,$$

where terms of order h^3 and higher have been neglected and $u_n(t) = u(nh, t) = u(x_n, t) = u(x, t)$ and $y_n(t) = y(nh, t) = y(x_n, t) = y(x, t)$. We now consider the scaled variables $\phi = \frac{\tilde{\chi}}{\sqrt{J\zeta}} u$, $\rho = \frac{\tilde{\chi}}{J} y$, $\tau = \frac{J}{\hbar} t$, and the scaled model parameter $\tilde{\beta} = \beta \frac{J^2}{\tilde{\chi}^2}$. We also introduce $v_s^{-2} = \frac{\bar{\eta} J^2}{\zeta \hbar^2}$, where v_s is the sound velocity, to finally get the simplified system:

$$i\phi_t = -h^2\phi_{xx} + h^2\rho_x\phi, \tag{A.1}$$
$$v_s^{-2}\rho_{tt} = \rho_{xx} + 3h^2\tilde{\beta}\rho_x^2\rho_{xx} + \frac{h^2}{12}\rho_{xxxx} + h^2\left(|\phi|^2\right)_x, \tag{A.2}$$

where the temporal variable τ has been recycled by t and the wave function ϕ has been scaled by the factor $\sqrt{h}$ to retain the right second order approximation.

The continuum system (A.1)–(A.2) represents a Schrödinger equation coupled to a type of Boussinesq equation, which is actually a variant of the system found by Gaididei et al. [12] for

cubic lattice anharmonicities. It is immediately seen that the system (A.1)–(A.2) becomes linearly unstable for relatively large wave numbers, precisely corresponding to the continuous limit just developed.

To avoid the instability problem of the continuous system (A.1)–(A.2), we consider the unidirectional stable wave propagation by means of the Zabusky and Kruskal approximation [16], where the derivative terms in ρ are dealt to neglect one of the directions of propagation, as follows. Let us first introduce the traveling coordinate $\xi = x - v_s t$ and the temporal scaling $\tau = v_s h^2 t/24$ yielding

$$-iv_s\phi_\xi + i\frac{v_s h^2}{24}\phi_\tau = -h^2\phi_{\xi\xi} + h^2\rho_\xi\phi, \tag{A.3}$$

$$0 = \frac{h^2}{12}\rho_{\tau\xi} - \frac{h^4}{24^2}\rho_{\tau\tau} + \frac{h^2}{2}\rho_\xi^2\rho_{\xi\xi} + \frac{h^2}{12}\rho_{\xi\xi\xi\xi} + h^2\left(|\phi|^2\right)_\xi, \tag{A.4}$$

where $\tilde{\beta}$ is set to $1/6$ to get the proper order approximation. The extra term ϕ_ξ in Eq. (A.3) appears due to traveling effects in the Schrödinger equation (A.1).

Let us now introduce the change of variables $v = \rho_\xi$ and $\phi = \phi(\xi,\tau) = \exp i\left(\frac{v_s}{2h^2}\xi + \frac{6v_s}{h^4}\tau\right)\psi(\xi,\tau)$ to remove the extra term ϕ_ξ and to retain the proper second order terms. We finish our continuum limit approximation by taking second order terms in h and neglecting higher order terms to find

$$iV\psi_t = -\psi_{xx} + v\psi, \tag{A.5}$$

$$0 = v_t + 6v^2 v_x + v_{xxx} + \left(|\psi|^2\right)_x, \tag{A.6}$$

where, for simplicity, variables ξ and τ have been replaced by x and t, respectively. On the other hand, $V = v_s/24$ is an effective model parameter that is related with the localization of the wave function (for all of our numerics we will chose the value $V = 1$). We have also scaled ϕ by $\sqrt{12}$ to get a unitary coefficient in front of the coupling term of Eq. (A.6) [note that Eq. (A.5) is scale invariant in ψ].

References

[1] L.D. Landau, Über die Bewegung der Elektronen in Kristalgitter, Phys. Z. Sowjetunion 3 (1933) 644.
[2] S.I. Pekar, Issledovanija po Elektronnoj Teorii Kristallov, Gostekhizdat, Moskva, 1951.
[3] Th. Holstein, Studies of polaron motion: Part I. The molecular crystal model, Ann. Phys. 8 (1959) 325–342.
[4] Th. Holstein, Studies of polaron motion: Part II. The "small" polaron, Ann. Phys. 8 (1959) 343–389.
[5] A.S. Davydov, Theory of Molecular Exitons, Plenum Press, New York, 1971.
[6] A.S. Davydov, Solitons in molecular systems, Phys. Scr. 20 (1979) 387.
[7] A.S. Davydov, Solitons in Molecular Systems, 2nd ed., Reidel, Dordrecht, 1991.
[8] A.S. Davydov, N.I. Kislukha, Phys. Status Solidi B 59 (1973) 465.
[9] A.S. Davydov, A.V. Zolotariuk, Subsonic and supersonic solitons in nonlinear molecular chains, Phys. Scr. 30 (1984) 426.
[10] A.V. Zolotaryuk, K.H. Spatschek, A.V. Savin, Supersonic mechanisms for charge and energy transfers in anharmonic molecular chains, Phys. Rev. B 54 (1996) 266.
[11] A.V. Zolotaryuk, K.H. Spatschek, A.V. Savin, Bifurcation scenario of the Davydov–Scott self-trapping mode, Europhys. Lett. 31 (1995) 531.
[12] Y.B. Gaididei, P.L. Christiansen, S.F. Mingaleev, Bound states of envelope and Boussinesq solitons in anharmonic lattices, Phys. Scr. 51 (1995) 289.
[13] Luis A. Cisneros-Ake, José F. Solano Peláez, Bright and dark solitons in the unidirectional long wave limit for the energy transfer on anharmonic crystal lattices, Physica D 346 (2017) 20.
[14] E. Fermi, J.R. Pasta, S.M. Ulam, Studies of Nonlinear Problems, Los Alamos scientific laboratory report LA-1940, 1955.
[15] X. Wang, D.W. Brown, K. Lindenberg, B.J. West, Alternative formulation of Davydov's theory of energy transport in bimolecular systems, Phys. Rev. A 37 (1988) 3557.
[16] Richard S. Palais, The symmetries of solitons, Bull. Am. Math. Soc. 34 (1997) 339.
[17] G.L. Lamb, Elements of Soliton Theory, Wiley-Intersci. Ser. Pure Appl. Math., 1980.
[18] A. Ramani, B. Grammaticos, T. Bountis, The Painlevé property and singularity analysis of integrable and non-integrable systems, Phys. Rep. 180 (1989) 159.
[19] G.B. Whitham, Linear and Nonlinear Waves, Wiley-Intersci. Ser. Texts Monogr. Tracts, 1999.
[20] L.N. Trefethen, Spectral Methods in Matlab, SIAM, Philadelphia, 2000.
[21] Stephen C. Anco, Nestor Tchegoum Ngatat, Mark Willoughby, Interaction properties of complex modified Korteweg–de Vries (mKdV) solitons, Physica D 240 (2011) 1378.
[22] Luis A. Cisneros-Ake, A.A. Minzoni, Effect of hydrogen bond anharmonicity on supersonic discrete Davydov soliton propagation, Phys. Rev. E 85 (2012) 021925.